

https://doi.org/10.1130/G48276.1

Manuscript received 13 August 2020 Revised manuscript received 30 September 2020 Manuscript accepted 4 October 2020

Published online 12 January 2021

© 2021 Geological Society of America. For permission to copy, contact editing@geosociety.org.

# "Missing links" for the long-lived Macdonald and Arago hotspots, South Pacific Ocean

L. Buff<sup>1\*</sup>, M.G. Jackson<sup>1</sup>, K. Konrad<sup>2,3</sup>, J.G. Konter<sup>4</sup>, M. Bizimis<sup>5</sup>, A. Price<sup>1</sup>, E.F. Rose-Koga<sup>6</sup>, J. Blusztajn<sup>7</sup>, A.A.P. Koppers<sup>3</sup>, and Santiago Herrera<sup>8</sup>

- <sup>1</sup>Department of Earth Science, University of California, Santa Barbara, California 93106, USA
- <sup>2</sup>Department of Geoscience, University of Nevada, Las Vegas, Nevada 89154, USA
- <sup>3</sup>College of Earth, Ocean, and Atmospheric Sciences, University of Oregon, Corvallis Oregon 97331, USA
- <sup>4</sup>Department of Earth Sciences, University of Hawaii-Manoa, Honolulu, Hawaii 96822, USA
- <sup>5</sup>School of the Earth, Ocean, and Environment, University of South Carolina, Columbia, South Carolina 29208, USA
- <sup>6</sup>Laboratoire Magmas et Volcans, Université Clermont Auvergne, CNRS-IRD-OPGC, 63170 Aubière, France
- <sup>7</sup>Department of Marine Chemistry, Woods Hole Oceanographic Institution, Woods Hole, Massachusetts 02543, USA
- <sup>8</sup>Department of Biological Sciences, Lehigh University, Bethlehem, Pennsylvania 18015, USA

### **ABSTRACT**

The Cook-Austral volcanic lineament extends from Macdonald Seamount (east) to Aitutaki Island (west) in the South Pacific Ocean and consists of hotspot-related volcanic islands, seamounts, and atolls. The Cook-Austral volcanic lineament has been characterized as multiple overlapping, age-progressive hotspot tracks generated by at least two mantle plumes, including the Arago and Macdonald plumes, which have fed volcano construction for ~20 m.y. The Arago and Macdonald hotspot tracks are argued to have been active for at least 70 m.y. and to extend northwest of the Cook-Austral volcanic lineament into the Cretaceous-aged Tuvalu-Gilbert and Tokelau Island chains, respectively. Large gaps in sampling exist along the predicted hotspot tracks, complicating efforts seeking to show that the Arago and Macdonald hotspots have been continuous, long-lived sources of hotspot volcanism back into the Cretaceous. We present new major- and trace-element concentrations and radiogenic isotopes for three seamounts (Moki, Malulu, Dino) and one atoll (Rose), and new clinopyroxene  $^{40}\text{Ar}/^{39}\text{Ar}$  ages for Rose  $(24.81 \pm 1.02 \text{ Ma})$  and Moki  $(44.53 \pm 10.05 \text{ Ma})$ . All volcanoes are located in the poorly sampled region between the younger Cook-Austral and the older, Cretaceous portions of the Arago and Macdonald hotspot tracks. Absolute plate motion modeling indicates that the Rose and Moki volcanoes lie on or near the reconstructed traces of the Arago and Macdonald hotspots, respectively, and the 40Ar/39Ar ages for Rose and Moki align with the predicted age progression for the Arago (Rose) and Macdonald (Moki) hotspots, thereby linking the younger Cook-Austral and older Cretaceous portions of the long-lived (>70 m.y.) Arago and Macdonald hotspot tracks.

#### INTRODUCTION

Intraplate volcanism is thought to result from buoyantly upwelling mantle plumes that partially melt beneath a moving plate, thereby producing age-progressive "hotspot" volcanism (e.g., Morgan, 1971). Some plume-derived volcanic chains, such as the Hawaii-Emperor and Louisville chains (Pacific Ocean), are well defined with clear age progressions extending back to ca. 80 Ma (Sharp and Clague, 2006; Koppers et al., 2012; O'Connor et al., 2013). The Cook-Austral volcanic lineament in the South Pacific Ocean (hereafter Cook-Austral) is the manifestation of

at least two overlapping hotspot tracks: the Arago (also referred to as "Rurutu" or "Atiu" trend) and Macdonald hotspot tracks. Denser sampling may reveal that not all seamounts along the predicted path of the Cook-Austral hotspots relate to these hotspots, but samples from two seamounts presented in this study strengthen hotspot age progressions anchored by young volcanism at Macdonald and Arago Seamounts, respectively (Fig. 1; Turner and Jarrard, 1982; Chauvel et al., 1997; Bonneville et al., 2002; Finlayson et al., 2018; Konrad et al., 2018; Rose and Koppers, 2019). While Cook-Austral volcanism has been argued to be relatively short-lived (0–20 m.y.; Chauvel et al., 1997; Lassiter et al.,

2003), there is growing evidence that the mantle plumes responsible for Cook-Austral volcanism are long-lived features responsible for generating Pacific seamounts during the Cretaceous (Staudigel et al., 1991; Koppers et al., 2001, 2003, 2007; Konter et al., 2008; Finlayson et al., 2018; Konrad et al., 2018).

Using absolute plate motion models, Koppers et al. (2003, 2007) and Konter et al. (2008) showed that Cretaceous Pacific island chains, including the Tokelau and Tuvalu-Gilbert chains, were located over the Macdonald and Arago mantle plumes, respectively (Fig. 1). Konter et al. (2008) also showed geochemical similarities between the Cretaceous and Cook-Austral portions of these two hotspot tracks, strengthening the link between the younger and older segments of these hotspot tracks. Recently, Finlayson et al. (2018) and Konrad et al. (2018) showed that the Tuvalu chain captures the 50 Ma "bend" (temporally and morphologically similar to the Hawaii-Emperor Bend) of the proposed Arago hotspot, thereby strengthening the link between the younger Cook-Austral and older Cretaceous segments of this proposed long-lived hotspot. However, volcanoes sampling the 45-10 Ma portion of the Arago hotspot represent an uncharacterized gap in the hotspot track. In contrast to the Arago hotspot, the Hawaii-Emperor Bend portion of the proposed Macdonald hotspot track has not yet been identified, and it will be important for linking the more recent Cook-Austral and older Cretaceous Tokelau segments of this hotspot track. Thus, while there is growing evidence that the Macdonald and Arago hotspots have been active since at least ca. 70 Ma, critical

CITATION: Buff, L., et al., 2021, "Missing links" for the long-lived Macdonald and Arago hotspots, South Pacific Ocean: Geology, v. 49, p. 541–544, https://doi.org/10.1130/G48276.1

<sup>\*</sup>E-mail: lbuff@ucsb.edu

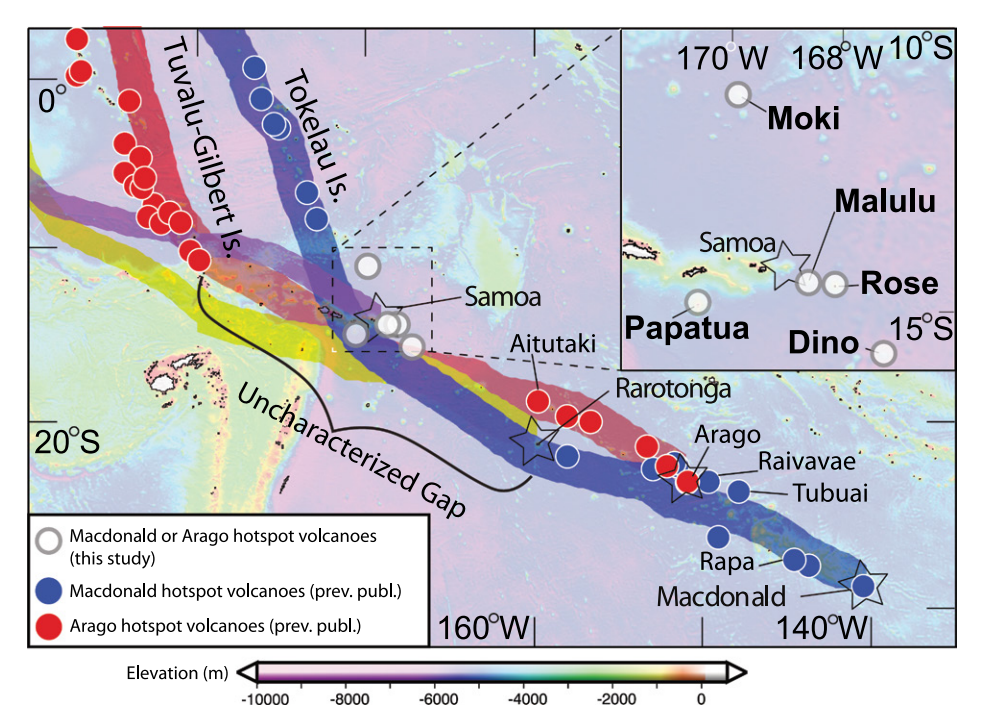


Figure 1. Map of current Cook-Austral, Tokelau, and Tuvalu-Gilbert Seamounts and volcanoes (South Pacific Ocean) pertaining to this study, showing reconstructed tracks for Samoan and Cook-Austral hotspots (including Macdonald and Arago hotspots). Shaded bands anchored to active portions of each hotspot track are reconstructed traces for each hotspot track (dark blue—Macdonald, red—Arago, yellow—Rarotonga, purple—Samoa) and are based on the absolute plate motion model of Wessel and Kroenke (2008); stars mark proposed hotspot locations. Blue circles represent volcanoes previously associated with the Macdonald hotspot, and red circles represent volcanoes previously associated with the Arago hotspot (data sources: Koppers et al., 2007; Konrad et al., 2018; Rose and Koppers, 2019; Jackson et al., 2020). Five interloper volcanoes investigated in this study are also indicated on this map: Moki, Malulu, Rose, Dino, and Papatua.

the Supplemental Material1). Descriptions and thin section images are publicly available for all EX1702 samples used in this study (osu-mgr. org/noaa-ex1702). We present new Sr-Nd-Pb-Hf isotopic data (Fig. 2; Fig. S1) and major- and trace-element concentrations (Fig. S2) on these volcanoes. The new geochemical and geochronological data, in conjunction with previously published geochemical data for two legacy samples from Rose Atoll and one legacy sample each for Malulu and Papatua Seamounts (obtained by deep-sea dredging; see Supplemental Materials; Jackson et al., 2010), show that the Moki and Rose volcanoes provide "missing links" between the younger Cook-Austral and older Cretaceous segments of the Macdonald and Arago hotspots, respectively. These links extend the longevity of the Arago and Macdonald hotspots to at least 70 Ma, making them two of the longest-lived hotspots in the Pacific Ocean.

### RESULTS AND DISCUSSION

Sample collection and analytical protocols for analysis of igneous material from Rose Atoll and the Malulu, Moki, and Dino Seamounts are detailed in the Supplemental Material. Due to the typically high degrees of submarine alteration,

<sup>1</sup>Supplemental Material. Methods, Figures S1–S3, and Tables S1–S4. Please visit https://doi.org/10.1130/GEOL.S.13377194 to access the supplemental material, and contact editing@geosociety.org with any questions.

gaps in sampling and characterization of these two hotspot tracks weaken the hypothesis for long-lived, continuous volcanism.

Volcanoes in the region of the Samoan hotspot track, located  $\sim$ 1000 km west-northwest of Aitutaki Island, were found to exhibit geochemical signatures inconsistent with nearby Samoan volcanoes (Jackson et al., 2010). Termed "interlopers" (i.e., not belonging in the region; Jackson et al., 2010), these volcanoes (Rose Atoll and two seamounts, Malulu and Papatua) yielded samples exhibiting significant alteration and thick ferromanganese coatings, which contrast with the young, fresh lavas from Samoan volcanoes in the region. These interloper volcanoes also exhibit geochemical signatures consistent with an origin over Cook-Austral hotspots, and the interloper volcanoes lie on, or close to, the reconstructed Macdonald and Arago hotspot traces.

We targeted the region between the Samoan hotspot and the Cook-Austral volcanic lineament for additional sampling on the National Oceanic and Atmospheric Administration (NOAA) ocean exploration cruise EX1702 aboard the *Okeanos Explorer* in February–March 2017. Four volcanoes were sampled (Rose Atoll and Malulu, Moki, and Dino Seamounts) by remotely operated vehicle (ROV; Fig. 1; Tables S1 and S2 in

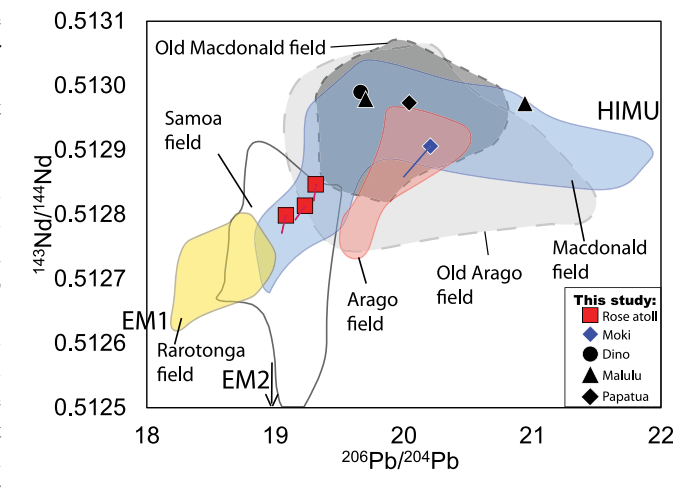


Figure 2. 143Nd/144Nd vs. <sup>206</sup>Pb/<sup>204</sup>Pb for volcanoes in this study plotted with existing data from Macdonald and Arago hotspot-related volcanoes (South Pacific Ocean). Moki and Malulu isotopic data produced for this study are from clinopyroxene phenocrysts, as seawater alteration prevented analysis of whole-rock samples. New data also include pillow rim glass analyses from Rose Atoll, whole-rock data from Dino Seamount, and whole-rock data from Rose, Malulu, and Papatua lavas previously

published by Jackson et al. (2010). Younger portions of the Arago (red field) and Macdonald (blue) hotspots in the Cook-Austral volcanic lineament are distinguished from older portions of these hotspots (light gray with long dashed lines for Tuvalu, Gilbert, Marshall, and Wake islands and seamounts [i.e., Old Arago]; dark gray with short dashed lines for Tokelau Islands and seamounts [i.e., Old Macdonald]). Age-corrected (to time of eruption) isotopic values are shown, but only where ages are available (Moki Seamount and Rose Atoll). Three undated Rose Atoll samples are assumed to have same age as sample EX1702-D3–2. Isotopic shift due to age correction is shown by line extending from respective data points (representing magnitude and direction of age correction). Other samples (Malulu, Papatua, and Dino) are not associated with ages, and age corrections are not provided. All data not produced in this study were previously published and downloaded from the Georoc database (http://georoc.mpch681mainz.gwdg.de/georoc). HIMU—high  $\mu$  = high  $^{238}$ U/ $^{204}$ Pb; EM1–EM2—enriched mantle sources. Figure is modified after Jackson et al. (2020).

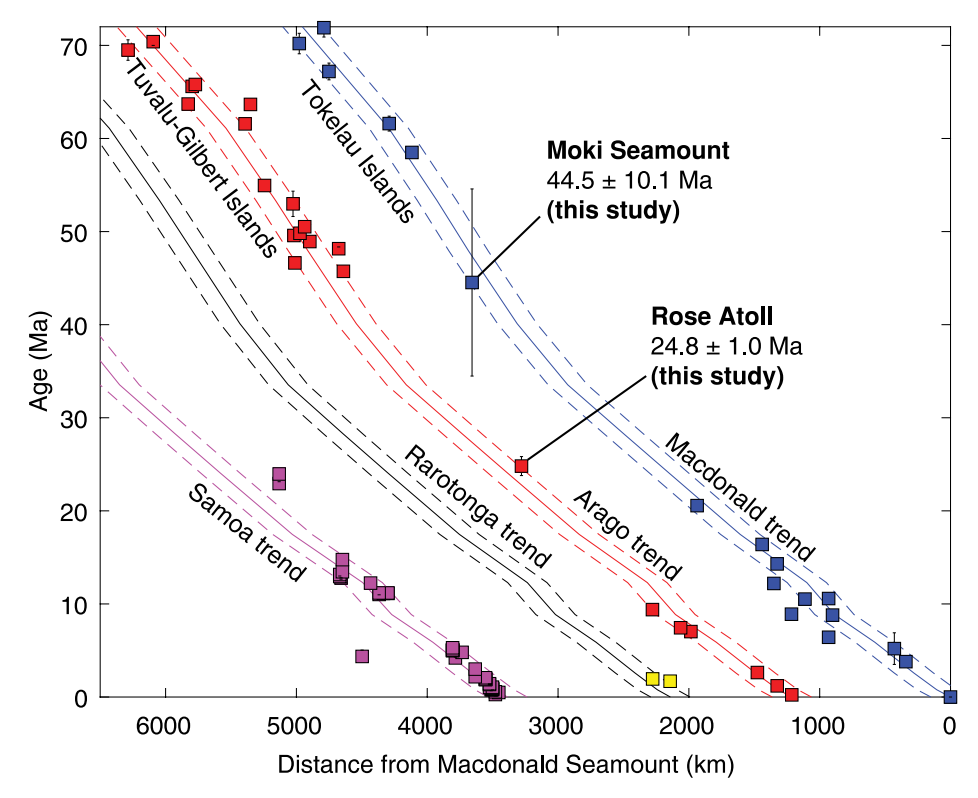


Figure 3. Hotspot track age-distance plot showing Rose and Moki volcanoes (South Pacific Ocean), including volcanoes associated with Macdonald, Arago, Rarotonga, and Samoa trends plotted along their respective reconstructed hotspot track. Clinopyroxene incremental-heating <sup>40</sup>Ar/<sup>39</sup>Ar ages for Rose and Moki are labeled (with 2 $\sigma$  uncertainties). Great circle distances from active hotspots were used. The absolute plate motion model of Wessel and Kroenke (2008), used to model volcanic age progressions, is shown for each hotspot (blue—Macdonald, red—Arago, black—Rarotonga, and pink—Samoa). Estimates for uncertainty in the Wessel and Kroenke (2008) model are also provided (dashed lines). Ages for Tokelau and Tuvalu-Gilbert volcanoes were published by Staudigel et al. (1991), Konter et al. (2008), Finlayson et al. (2018), and Konrad et al. (2018). Ages for Cook-Austral volcanic lineament were compiled by Jackson et al. (2020) and Rose and Koppers (2019).

fine-grained to glass-rich groundmasses, and/ or absence of traditionally dated phenocrystic phases (e.g., plagioclase), ages were not available for whole-rock samples from these five volcanoes; nonetheless, with extensive acid leaching, we could obtain radiogenic isotopic compositions on these samples (see the Supplemental Material). However, new advancements in 40Ar/39Ar methodology permit age determinations from clinopyroxene phenocrysts (Konrad et al., 2019). Using this technique, we successfully dated lava flows from the Moki and Rose volcanoes. The clinopyroxene separates from Rose Atoll (sample AVON2/3-D66-1) and Moki Seamount (sample EX1702-D7-2) both produced age spectra that met standard 40Ar/39Ar criteria, where plateaus included >60% of the  $^{39}Ar_{(K)}$ , and probability of fit (P) values were >5%. Two experiments for AVON2/3-D66–1, carried out on two clinopyroxene size fractions, produced concordant plateaus, which allowed the results to be combined and averaged (Fig. S3). The 40Ar/36Ar intercept values are within uncertainty of atmosphere (298.6), supporting the plateau age of 24.81  $\pm$  1.02 Ma (2 $\sigma$ ). This age places Rose Atoll squarely on the age progression for the Arago hotspot (Fig. 3), which is consistent with the observation that Rose Atoll is near the reconstructed trace of the Arago hotspot (Fig. 1). Sample EX1702-D7–2 contained low concentrations of potassium-derived <sup>39</sup>Ar and radiogenic <sup>40</sup>Ar, resulting in large uncertainties. The experiment produced a long plateau with a slightly higher-than-atmospheric <sup>40</sup>Ar/<sup>36</sup>Ar intercept value of  $313 \pm 12 \ (2\sigma)$ . Therefore, the inverse isochron age determination is preferred at  $44.53 \pm 10.05 \ \text{Ma} \ (2\sigma) \ (\text{Fig. S3}; \text{Tables S3} \ \text{and S4})$ . While uncertainties are large, the Moki Seamount age places it on the Macdonald hotspot age progression (Fig. 3).

New geochemical data are presented in Tables S1 and S2. In radiogenic isotopic space, Macdonald and Arago Seamounts sampled HIMU (high  $\mu=$  high  $^{238}\text{U}/^{204}\text{Pb}$ ), enriched mantle (EM), and geochemically depleted end members (Chauvel et al., 1992, 1997; Lassiter et al., 2003; Hanyu et al., 2013) that may reflect a contribution from a common (C; Hanan and Graham, 1996) component or a FOZO (Hart et al., 1992) component (Konter et al., 2008; Fig. 2; Fig. S1). While Rose Atoll erupted over the Arago hotspot, whole-rock (Jackson et al.,

2010) and glass geochemistry does not consistently plot in the fields for Arago hotspot volcanoes in the Cook-Austral volcanic lineament or the older portion of the Arago hotspot (Gilbert, Tuvalu, Marshall, and Wake islands and seamounts), and in some isotope spaces, one or multiple Rose samples plot only in the field for Macdonald hotspot volcanoes (Fig. 2; Fig. S1).

The Moki Seamount sample yielded an age with greater uncertainty, but the age is nonetheless consistent with a Macdonald hotspot origin, and the Moki sample consistently falls in a region of isotopic space that overlaps with Macdonald hotspot volcanoes (Fig. 2; Fig. S1). In the hotspot reconstruction using the Wessel and Kroenke (2008) absolute plate motion model, Moki plots significantly closer to the reconstructed trace of the Macdonald hotspot track than the Arago hotspot track, consistent with the geochronological and geochemical data provided here (Fig. 1). While uncertainties are large, the Moki Seamount age places it on the Macdonald hotspot age progression (Fig. 3), and the age for Moki overlaps with the reconstructed Macdonald hotspot track, even at the  $1\sigma$  level.

The Dino Seamount sample and the new Malulu Seamount sample presented here (EX1702-D12-5) consistently plot in the field for Macdonald hotspot volcanoes in the Cook-Austral volcanic lineament, but age data are needed before a Macdonald hotspot designation can be assigned. Papatua Seamount (Jackson et al., 2010) plots in a region that overlaps the Macdonald and Arago hotspots in all isotopic spaces for which there are available data, except for the 206Pb/204Pb versus 143Nd/144Nd isotope space, where it plots in the Macdonald field (Fig. 2; Fig. S1). Unfortunately, Papatua is also geographically located on a portion of the reconstructed hotspot tracks where the Macdonald and Arago tracks overlap, preventing a hotspot designation for Papatua. Age data are needed to determine the hotspot origin of this seamount.

The link between the younger Cook-Austral and older Cretaceous segments of the Macdonald and Arago hotspots provided by samples from Moki Seamount and Rose Atoll, respectively, has two key implications: (1) it allows us to posit, with greater confidence, that the Macdonald hotspot is both continuous and long-lived, and (2) it supports previous arguments for the longevity of the Arago hotspot (Finlayson et al., 2018). Thus, the Macdonald and Arago hotspots join Hawaii (Tarduno et al., 2003; O'Connor et al., 2013) and Louisville (Lonsdale, 1988; Koppers et al., 2012) as two Pacific hotspots for which activity has been mapped for least 70 m.y.

An important outcome of this work is the strengthening of the case for the longevity of the Arago and Macdonald hotspots. However, it is becoming increasingly clear that the Arago and Macdonald hotspots show significant

overlap in Sr-Nd-Pb-Hf isotopic space, and it is the combination of geochemistry and ages that uniquely constrains the hotspot to which a given seamount belongs. For example, the Arago and Macdonald plumes have consistently sampled the most extreme HIMU compositions (206Pb/204Pb up to 21.42 for Arago, and 21.93 for Macdonald; Fig. 2) in the Pacific since the Cretaceous (Konter et al., 2008; Hanyu et al., 2011; Finlayson et al., 2018). The reason for this may be due to the close proximity of the two hotspots: The long-lived Arago hotspot is located just  $\sim$ 1200 km west-northwest from the Macdonald hotspot. If both hotspots are fed by mantle plumes that emerge from the core-mantle boundary, the plume conduits are separated by only  $\sim$ 660 km at the core-mantle boundary. Thus, the regions (i.e., "feeding zones") at the core-mantle boundary that are sourcing material to the upwelling Macdonald and Arago plumes may overlap, explaining the similar isotopic signatures at both hotspots (Fig. 2). If both plumes have been producing active volcanism for >70 m.y., an important dynamic question to be addressed is how the two closely spaced plume conduits have interacted over geologic time (Lassiter et al., 2003). Both plumes arise from the large low-shear-wave-velocity province (LLSVP) situated on top of the core-mantle boundary beneath the Pacific (Jackson et al., 2018), and long-lived HIMU signatures in both plumes might suggest that this is a geochemical characteristic of the region of the Pacific LLSVP that is sourced by both plumes.

### ACKNOWLEDGMENTS

We acknowledge helpful reviews from Oliver Nebel and two anonymous reviewers. We thank the National Oceanic and Atmospheric Administration (NOAA) Ocean Explorer program and the crew of the Okeanos Explorer expedition EX1702. The Oregon State University Marine and Geology Repository provided samples from the EX1702 expedition. Buff thanks V. Finlayson for her assistance with the Arago and Tuvalu-Gilbert data sets. Konrad thanks D. Heaton for assistance with the age determinations. Jackson acknowledges support from National Science Foundation grants OCE-1912931, EAR-1900652, and EAR-1429648. Rose-Koga acknowledges support from Laboratory of Excellence ClerVolc (Clermont-Ferrand Centre for Volcano Research). This is Laboratory of Excellence ClerVolc contribution 438.

### REFERENCES CITED

- Bonneville, A., Le Suave, R., Audin, L., Clouard, V., Dosso, L., Gillot, P.Y., Janney, P., and Maamaatuaiahutapu, K., 2002, Arago Seamount: The missing hotspot found in the Austral Islands: Geology, v. 30, p. 1023–1026, https://doi.org/10.1130/0091-7613(2002)030<1023:AST MHF>2.0.CO;2.
- Chauvel, C., Hofmann, A.W., and Vidal, P., 1992, HIMU-EM: The French Polynesian connection: Earth and Planetary Science Letters, v. 110, p. 99–119, https://doi.org/10.1016/0012-821X(92)90042-T.
- Chauvel, C., McDonough, W., Guille, G., Maury, R., and Duncan, R., 1997, Contrasting old and young volcanism in Rurutu Island, Austral chain:

- Chemical Geology, v. 139, p. 125–143, https://doi.org/10.1016/S0009-2541(97)00029-6.
- Finlayson, V., Konter, J.G., Konrad, K., Koppers, A.A.P., Jackson, M.G., and Rooney, T.O., 2018, Sr-Pb-Nd-Hf isotopes and 40Ar/30Ar ages reveal a Hawaii-Emperor-style bend in the Rurutu hotspot: Earth and Planetary Science Letters, v. 500, p. 168–179, https://doi.org/10.1016/j.epsl.2018.08.020.
- Hanan, B.B., and Graham, W.D., 1996, Lead and helium isotope evidence from oceanic basalts for a common deep source of mantle plumes: Science, v. 272, p. 991–995, https://doi.org/10.1126/science.272.5264.991.
- Hanyu, T., Tatsumi, Y., Senda, R., Miyazaki, T., Chang, Q., Hirahara, Y., Takahashi, T., Kawabata, H., Suzuki, K., Kimura, J., Nakai, S., 2011, Geochemical characteristics and origin of the HIMU reservoir: A possible mantle plume source in the lower mantle: Geochemistry Geophysics Geosystems, v. 12, Q0AC09, https://doi .org/10.1029/2010GC003252.
- Hanyu, T., Dosso, L., Ishizuka, O., Tani, K., Hanan, B.B., Adam, C., Nakai, S., Senda, R., Chang, Q., and Tatsumi, Y., 2013, Geochemical diversity in submarine HIMU basalts from Austral Islands, French Polynesia: Contributions to Mineralogy and Petrology, v. 166, p. 1285–1304, https://doi.org/10.1007/s00410-013-0926-x.
- Hart, S.R., Hauri, E.H., Oschmann, L.A., and Whitehead, J.A., 1992, Mantle plumes and entrainment: Isotopic evidence: Science, v. 256, p. 517–520, https://doi.org/10.1126/science.256.5056.517.
- Jackson, M.G., Hart, S.R., Konter, J.G., Koppers, A.A.P., Staudigel, H., Kurz, M.D., Blusztajn, J., and Sinton, J.M., 2010, The Samoan hotspot track on a "hotspot highway": Implications for mantle plumes and a deep Samoan mantle source: Geochemistry Geophysics Geosystems, v. 11, Q12009, https://doi.org/10.1029/2010GC003232.
- Jackson, M.G., Becker, T.W., and Konter, J.G., 2018, Geochemistry and distribution of recycled domains in the mantle inferred from Nd and Pb isotopes in oceanic hot spots: Implications for storage in the large low shear wave velocity provinces: Geochemistry Geophysics Geosystems, v. 19, p. 3496–3519, https://doi .org/10.1029/2018GC007552.
- Jackson, M.G., Halldórsson, S.A., Price, A., Kurz, M.D., Konter, J.G., Koppers, A.A.P., Day, J.M.D., 2020, Contrasting old and young volcanism from Aitutaki, Cook Islands: Implications for the origins of the Cook-Austral volcanic chain: Journal of Petrology, v. 61, no. 3, p. egaa037, https://doi .org/10.1093/petrology/egaa037.
- Konrad, K., Koppers, A.A.P., Steinberger, B., Finlayson, V., Konter, J., and Jackson, M.G., 2018, On the relative motions of long-lived Pacific mantle plumes: Nature Communications, v. 9, p. 854, https://doi.org/10.1038/s41467-018-03277-x.
- Konrad, K., Koppers, A.A., Balbas, A.M., Miggins, D.P., and Heaton, D.E., 2019, Dating clinopyroxene phenocrysts in submarine basalts using <sup>40</sup>Ar/<sup>39</sup>Ar geochronology: Geochemistry Geophysics Geosystems, v. 20, p. 1041–1053, https:// doi.org/10.1029/2018GC007697.
- Konter, J.G., Hanan, B.B., Blichert-Toft, J., Koppers, A.A.P., Plank, T., and Staudigel, H., 2008, One hundred million years of mantle geochemical history suggest the retiring of mantle plumes is premature: Earth and Planetary Science Letters, v. 275, p. 285–295, https://doi.org/10.1016/ j.epsl.2008.08.023.
- Koppers, A.A.P., Phipps Morgan, J., and Staudigel, H., 2001, Testing the fixed hotspot hypothesis using <sup>40</sup>Ar/<sup>39</sup>Ar age progressions along seamount trails: Earth and Planetary Science Let-

- ters, v. 185, p. 237–252, https://doi.org/10.1016/S0012-821X(00)00387-3.
- Koppers, A.A.P., Pringle, M.S., and Wijbrans, J.R., 2003, Short-lived and discontinuous intraplate volcanism in the South Pacific: Hot spots or extensional volcanism?: Geochemistry Geophysics Geosystems, v. 4, 1089, https://doi .org/10.1029/2003GC000533.
- Koppers, A.A.P., Staudigel, H., Phipps Morgan, J., and Duncan, R.A., 2007, Nonlinear <sup>40</sup>Ar/<sup>39</sup>Ar age systematics along the Gilbert Ridge and Tokelau Seamount trail and the timing of the Hawaii-Emperor Bend: Geochemistry Geophysics Geosystems, v. 8, Q06L13, https://doi.org/10.1029/2006GC001489.
- Koppers, A.A.P., et al., 2012, Limited latitudinal mantle plume motion for the Louisville hotspot: Nature Geoscience, v. 5, p. 911–917, https://doi.org/10.1038/ngeo1638.
- Lassiter, J.C., Blichert-Toft, J., Hauri, E.H., and Barsczus, H.G., 2003, Isotope and trace element variations in lavas from Raivavae and Rapa, Cook-Austral islands: Constraints on the nature of HIMU- and EM-mantle and the origin of mid-plate volcanism in French Polynesia: Chemical Geology, v. 202, p. 115–138, https:// doi.org/10.1016/j.chemgeo.2003.08.002.
- Lonsdale, P., 1988, Geography and history of the Louisville hotspot chain in the southwest Pacific: Journal of Geophysical Research, v. 93, p. 3078–3104, https://doi.org/10.1029/JB093iB04p03078.
- Morgan, W.J., 1971, Convection plumes in the lower mantle: Nature, v. 230, p. 42–43, https://doi.org/10.1038/230042a0.
- O'Connor, J.M., Steinberger, B., Regelous, M., Koppers, A.A.P., Wijbrans, J.R., Haase, K.M., Stoffers, P., Jokat, W., and Garbe-Schönberg, D., 2013, Constraints on past plate and mantle motion from new ages for the Hawaiian-Emperor Seamount Chain: Geochemistry Geophysics Geosystems, v. 14, p. 4564–4584, https://doi.org/10.1002/ggge.20267.
- Rose, J., and Koppers, A.A.P., 2019, Simplifying age progressions within the Cook-Austral Islands using high-resolution ARGUS-VI <sup>40</sup>Ar/<sup>39</sup>Ar incremental heating ages: Geochemistry Geophysics Geosystems, v. 20, p. 4756–4778, https://doi.org/10.1029/2019GC008302.
- Sharp, W.D., and Clague, D.A., 2006, 50-Ma initiation of Hawaiian-Emperor Bend records major change in Pacific plate motion: Science, v. 313, p. 1281–1284, https://doi.org/10.1126/science.1128489.
- Staudigel, H., Park, K.-H., Pringle, M., Rubenstone, J.L., Smith, W.H.F., and Zindler, A., 1991, The longevity of the South Pacific isotopic and thermal anomaly: Earth and Planetary Science Letters, v. 102, p. 24–44, https://doi.org/10.1016/0012-821X(91)90015-A.
- Tarduno, J.A., Duncan, R.A., Scholl, D.W., Cottrell, R.D., Steinberger, B., Thordarson, T., Kerr, B.C., Neal, C.R., Frey, F.A., Torii, M., and Carvallo, C., 2003, The Emperor Seamounts: Southward motion of the Hawaiian hotspot plume in Earth's mantle: Science, v. 301, p. 1064–1069, https://doi .org/10.1126/science.1086442.
- Turner, D.L., and Jarrard, R.D., 1982, K/Ar dating of the Cook Austral island chain; a test of the hot spot hypothesis: Journal of Volcanology and Geothermal Research, v. 12, p. 187–220, https://doi.org/10.1016/0377-0273(82)90027-0.
- Wessel, P., and Kroenke, L.W., 2008, Pacific absolute plate motion since 145 Ma: An assessment of the fixed hot spot hypothesis: Journal of Geophysical Research, v. 113, B06101, https://doi.org/10.1029/2007JB005499.

Printed in USA

# Supplemental Materials

### Methods

Sample locations, preparation and wet chemistry.

The samples in this study were collected by deep submarine dredging from four seamounts (Papatua, Moki, Seamount D ["Dino"], Malulu) and one atoll (Rose) in the Samoan region. Several samples in this study were collected during the 2017 expedition (EX1702) aboard the NOAA *Okeanos Explorer*: Moki seamount (basaltic sample D7-2), Dino seamount (basaltic sample D11-1), Rose atoll (pillow fragment sample D3-2), and Malulu seamount (hyaloclastite sample D12-5). Finally, two samples from the 1999 AVON2/3 expedition aboard the R/V Melville which were previously characterized are presented here with modern Pb-isotopic analyses: AVON2/3-D67-11 from Malulu seamount which is an altered basalt, and basaltic sample AVON2/3-D66-1 from Rose atoll. Tables S1 and S2 present previously published data on these two Rose samples in addition to two other samples—AVON2/3-D65-18 (from Malulu seamount) and ALIA-DR129-05 (from Papatua seamount) —from non-Samoan seamounts in the Samoan region. Sample locations and geochemical characterization of these four previously published lavas can be found in **Jackson et al. (2010)**.

Samples were crushed in plastic bags to avoid exposure to metal. Crushed material was then sieved. For two samples (EX1702-D12-5 hyaloclastite from Malulu seamount and EX1702-D7-2 basalt from Moki seamount), clinopyroxene was removed for radiogenic isotopic work due to the lack of fresh basaltic material. For Rose atoll sample EX1702-D3-2, volcanic glass was removed from the pillow rim for radiogenic isotopic analysis (this glass was also characterized for major and trace element compositions, but we also present whole rock major and trace element data for this sample as well). For sample EX1702-11-1 (Seamount D), 200 mg of the freshest (0.5 to 1 mm) rock chips were analyzed, targeting groundmass. We also separated the freshest groundmass chips from two previously characterized lavas—AVON2/3-D66-1 (Rose atoll) and AVON2/3-D67-11 (Malulu seamount)—for a new characterization using modern Pb isotopic analyses and new analyses of Sr and Nd isotopes on the same material.

The groundmass samples (including the EX1702-D3-2 glass) were treated with a heavy leaching protocol described in **Price et al. (2016)** which, in addition to the 6N HCl leaching treatment, uses hot 4N HNO<sub>3</sub> and hot 30% H<sub>2</sub>O<sub>2</sub>. The clinopyroxene samples were first leached in concentrated HCl on a hot plate for 1 hour at 40° C, then in concentrated nitric for 1 hour at 40° C, with ~1 hour of sonication in the same acid following each leaching step; after this initial leach, the clinopyroxenes were subjected to the same "heavy leaching" as the groundmass and glass samples (and, following leaching, only pristine clinopyroxenes were selected for dissolution and analysis). Note that replicated analysis of the D11-1 groundmass followed additional leaching: it was treated with the strong leaching protocol followed by an additional 8 hours of leaching in 6N HCl at 60° C and an additional 10 minutes leaching in cold concentrated HF; this may explain the offset in Sr, Nd, and Pb isotopes between the original and replicate rounds of analyses of this sample. USGS reference materials were not leached. Following leaching, samples were rinsed and sonicated repeatedly in MilliQ H<sub>2</sub>O ( $\geq$  18.2 M $\Omega$  · cm deionized water). Sample dissolution, wet chemistry (including Sr, Pb, Hf and Nd elemental separations), and mass spectrometry was carried out in one of the three following institutions:

1. One batch of samples underwent Sr, Nd, and Pb chemical separations at UCSB, with Sr and Nd isotopes analyzed on the UCSB TIMS and Pb isotopes analyzed on the WHOI

MC-ICP-MS; the wet chemistry follows methods developed in **Price et al. (2014)** with modifications as follows: Following dissolution in concentrated HF and HNO<sub>3</sub>, Sr and Pb were purified by two passes through 100  $\mu$ L of Eichrom Sr resin (25-50  $\mu$ m), and Nd purified was purified from the wash of the Sr resin using a two-step method employing Eichrom TRU resin (100-150  $\mu$ m) followed by Eichrom LN-Spec resin (50-100  $\mu$ m). Total procedural blanks are <200 pg for Sr, <50 pg for Nd, and < 120 pg for Pb.

- 2. A second batch of samples underwent Sr, Nd, and Pb chemical separations at UCSB as described above, with Sr and Nd isotopes analyzed on the UCSB TIMS. However, Pb isotopes were analyzed on the University of South Carolina MC-ICP-MS.
- 3. A third batch of samples, which included just the cpx separates for EX1702-D12-5 and EX1702-D7-5, underwent dissolution, chemical separations (for Sr, Nd, Hf, and Pb), and mass spectrometry at the University of South Carolina.

Further description of wet chemistry and mass spectrometry is provided below.

Sr and Nd mass spectrometry at UCSB and Pb mass spectrometry at WHOI.

Sr and Nd isotopes were analyzed on a Thermo Triton Plus TIMS mass spectrometer housed at UCSB. 500 ng of Sr or Nd was loaded on outgassed, zone-refined Re (99.999% purity, H-Cross, USA) filaments. With the exception of the first <sup>87</sup>Sr/<sup>86</sup>Sr analyses (EX1702-D12-5 clinopyroxene, EX1702-D7-5 clinopyroxene, EX1702-D11-1, EX1702-D3-2) and associated standards, which used a 33 picoamp gainboard but did not employ amplifier rotation, all other Sr and Nd isotopic analyses of samples, replicates, and associated standards employed amplifier rotation on 10<sup>11</sup> ohm amplifiers and a 3.3 picoamp gainboard. Gains were run with the start of a new barrel. Approximately 20% of analysis time was devoted to baselines: baselines are taken with each rotation of the amplifiers (i.e., because 5 amplifiers-cup pairs were used during analyses, 5 baselines were taken during each full amplifier rotation). Intensities were kept at approximately 3V on mass 88 and 3V on mass 144 during 87Sr/86Sr and 143Nd/144Nd analyses. respectively. Sr and Nd isotopes were corrected for mass bias assuming an exponential law and using canonical <sup>86</sup>Sr/<sup>88</sup>Sr and <sup>146</sup>Nd/<sup>144</sup>Nd ratios of 0.1194 and 0.7219, respectively. Isobaric interferences from Rb and Sm were corrected by monitoring masses 85 and 147, but corrections to the <sup>87</sup>Sr/<sup>86</sup>Sr and <sup>143</sup>Nd/<sup>144</sup>Nd ratios were nominal. USGS reference materials (processed through all steps of wet chemistry and column chemistry with unknowns at UCSB) and sample unknowns were corrected for the offset between preferred and measured standard (NBS987 or JNdi) values with each barrel: preferred value for NBS987 87Sr/86Sr is 0.710240, and JNdi is 0.512099 (Garçon et al., 2018). On the UCSB Triton Plus the average 87Sr/86Sr and 143Nd/144Nd and long-term reproducibility, up to and including this study, of NBS987 and JNdi using amplifier rotation is  $0.710246 \pm 0.000011$  (2SD, N=29) and,  $0.512100 \pm 0.000004$  (2SD, N=27), respectively. The corresponding average <sup>87</sup>Sr/<sup>86</sup>Sr and long-term reproducibility when analyzing NBS987 without amplifier rotation is  $0.710244 \pm 0.000014$  (2SD, N=39).

We note that prior analyses of the AVON2/3 cruise samples from Rose (AVON2/3-D66-1) and Malulu (AVON2/3-D67-11), reported in **Jackson et al. (2010)**, should be replaced by new analyses of these two samples shown in **Table S1**, for two reasons: 1) the previously published Pb isotopic analyses were made by TIMS without a spike addition to control for in-run mass fractionation and 2) these two samples exhibit significant alteration and acid leaching for the prior analyses may not have been sufficient to have removed alteration phases. We note that the new <sup>143</sup>Nd/<sup>144</sup>Nd analysis for AVON2/3-D67-11 (0.512982) shows significant disagreement with the prior analysis (0.512796, after correction to the JNdi reference frame use here by

applying the La Jolla to JNdi conversion from **Tanaka et al., 2000**) made at WHOI in the year 2000 and reported by **Jackson et al. (2010)**. In order to evaluate the accuracy of the new <sup>143</sup>Nd/<sup>144</sup>Nd measurement, three additional aliquots of this sample were obtained from the WHOI dredge repository, including the original bag of crushed rock chips for this sample from which material was extracted for the 2000 analysis (see AVON2/3-D67-11 rep1, rep2, and rep3 in **Table S1**); new batches of chips were prepared by separately crushing each aliquot, and the different aliquots of chips were leached and underwent wet chemistry and mass spectrometry during a separate session than the original analyses. The three replicate <sup>143</sup>Nd/<sup>144</sup>Nd analyses (0.512982, 0.512980, and 0.512981) show excellent agreement with the new <sup>143</sup>Nd/<sup>144</sup>Nd result, confirming its accuracy. We note that the new analyses of Sr and Pb isotopes for this sample are similar to the published data for this sample reported in **Jackson et al. (2010)**.

Using the Pb fractions purified at UCSB, Pb isotopic analyses were carried out at the Woods Hole Oceanographic Institution using the Thermo Neptune MC-ICP-MS housed there (**Hart and Blusztajn, 2006**). Fractionation correction was made by Tl-addition assuming an exponential fractionation law (**White et al., 2001**). Samples and an aliquot of AGV-2 (processed through all steps of column chemistry and mass spectrometry with the samples) were corrected for the offset between preferred (i.e., values from **Eisele et al., 2003**; ( $^{206}$ Pb/ $^{204}$ Pb = 16.9409,  $^{207}$ Pb/ $^{204}$ Pb = 15.4976, and  $^{208}$ Pb/ $^{204}$ Pb = 36.7262)) and measured ratios of NBS981.

For a different subset of samples (specified in **Table S2**), Pb fractions purified at UCSB were carried out at the University of South Carolina on Thermo Neptune MC-ICP-MS housed there. The samples, together with an aliquot of BCR-2 (processed through all steps of column chemistry and mass spectrometry with the samples) were corrected for the offset between preferred (i.e., values from **Eisele et al., 2003**) and measured ratios of NBS981.

Sr, Nd, Hf and Pb isotopic and major and trace element concentrations on clinopyroxenes from samples EX1702-D12-5 and EX1702-D7-5 at U. South Carolina.

Following leaching, visually fresh clinopyroxenes were picked under a binocular microscope. The clinopyroxene samples were then processed at the Center for Elemental Mass Spectrometry, University of South Carolina. Approximately 150-200 mg of sample was first leached (using the same protocol described above) and dissolved in Teflon distilled HF:HNO3 (3:1) mixture on a hot plate for ~ 3 days, with frequent sonication. After drydown the samples were picked in 6N HCl with added boric acid in 10N HCl to complex fluorides, which increases yields in Hf chemistry (Frisby et al., 2016). Afterwards the samples were converted to nitrates. A small aliquot (~5%) was taken for Sr and Nd isotopes and the remainder was dried down with HBr for Pb and then Hf chemistry. A precisely determined aliquot of the dissolved clinopyroxene samples was pipetted from the solution and gravimetrically diluted for trace element analyses prior to the splitting of Sr-Nd and Pb-Hf fractions. Trace elements were then analyzed by ICP-MS with an aliquot of BHVO-1 on the Element2 following established methods for the lab (e.g. Frisby et al, 2016).

For the chemical separations, Sr was separated first on an Eichrom Sr-spec resin and the washes containing the rest of the elements were processed through an Eichrom TRU spec resin to concentrate the LREEs, and then on an Eichrom Ln-Resin to isolate Nd (**Frisby et al, 2016**). The Pb was separated on anion resin in HBr and HCl media, and the washes from that were processed for Hf following the method of **Munker et al. (2001**). An unleached BCR-2 powder was dissolved and processed through all steps of chemistry and mass spectrometry with sample unknowns. Total procedural blanks during the analytical session were 10 pg for Pb, 180 pg for

Sr, <10 pg for Nd, and 40 pg for Hf.

The isotopic compositions of Sr, Nd, Pb, and Hf were measured on the Thermo Neptune housed at the University of South Carolina following methods provided in **Beguelin et al.**, **(2017)**. All samples were corrected for mass bias using the exponential law: Pb was corrected using the Tl addition method (**White et al., 2001**), <sup>87</sup>Sr/<sup>86</sup>Sr was corrected using <sup>86</sup>Sr/<sup>88</sup>Sr of 0.1194, <sup>143</sup>Nd/<sup>144</sup>Nd was corrected using <sup>146</sup>Nd/<sup>144</sup>Nd of 0.7219, and <sup>176</sup>Hf/<sup>177</sup>Hf was corrected using <sup>179</sup>Hf/<sup>177</sup>Hf of 0.7325. All isotopic data on samples were corrected for the offset between measured and preferred standards using the following preferred values: SRM981 values from **Eisele et al. (2003)**; NBS987 <sup>87</sup>Sr/<sup>86</sup>Sr value of 0.710240; JMC-475 <sup>176</sup>Hf/<sup>177</sup>Hf value of 0.282160; JNdi <sup>143</sup>Nd/<sup>144</sup>Nd value of 0.512099 (**Garçon et al., 2018**).

During the course of these measurements, reproducibility of <sup>87</sup>Sr/<sup>86</sup>Sr on NBS987 was 22 ppm, of <sup>143</sup>Nd/<sup>144</sup>Nd on JNdi-1 was 20 ppm, of <sup>176</sup>Hf/<sup>177</sup>Hf on JMC-475 was 28 ppm, and Pb isotopic compositions on NBS981 were 62ppm on <sup>206</sup>Pb/<sup>204</sup>Pb, 68 ppm for <sup>207</sup>Pb/<sup>204</sup>Pb, and 80 ppm for <sup>208</sup>Pb/<sup>204</sup>Pb (all 2SE). An unleached BCR-2 powder was run together with the clinopyroxenes through all steps of column chemistry and mass spectrometry, and data are shown in **Table S1**.

Whole rock major and trace element analyses at Washington State University.

For samples EX1702-D7-2, EX1702-D3-2, and EX1702-D11-1, 10 to 20 g blocks of rock were cut with the rock saw, and care was taken to avoid visibly altered portions of rock. The blocks were cleaned with silicon carbide sand paper, and sonicated in MilliQ H<sub>2</sub>O. Samples were crushed and then powdered in an agate shatterbox (with cleaning with silica between barrels) at the Geoanalytical lab at the Washington State University (WSU). Major and trace element concentrations were obtained at WSU by X-ray fluorescence (XRF) and ICP-MS. XRF and ICP-MS methods, and evaluation of accuracy using international standards, are reported elsewhere (Knaack et al., 1994; Johnson et al., 1999), but summarized briefly here. The precision  $(1\sigma)$  for major elements in basalts by XRF is 0.11–0.33% (1σ) of the amount present for SiO<sub>2</sub>, Al<sub>2</sub>O<sub>3</sub>, TiO<sub>2</sub>, P<sub>2</sub>O<sub>5</sub>) and 0.38–0.71% for other elements. Trace element precision of basalts by ICP-MS is 0.77–3.2% (1 $\sigma$ ) for trace elements except for U (9.3%) and Th (9.5%). An aliquot of the USGS reference material BCR-2 was analyzed as an unknown together with the basaltic unknowns, and the data are reported in **Table S2**. The new analysis of BCR-2 reported here is compared to major and trace element compositions for this reference material reported in **Jochum et al.** (2016). Whole rock major and trace element analyses of the AVON2/3-D67-1, AVON2/3-D66-1, AVON2/3-D65-18 and ALIA-DR129-05 were made following the same methods and data are reported in Jackson et al. (2010).

In situ major element analyses on glass by electron microprobe at UC Santa Barbara.

Glass was available for EX1702-D3-2. Sample chips were analyzed by electron microprobe at UC Santa Barbara using primary standards and following analytical conditions outlined in **Jackson et al. (2015)**. The MORB basaltic secondary standard 519-4-1 was analyzed repeatedly throughout the analytical session. Major element compositions for sample unknown glass and the secondary standard (and previously published data on this secondary standard from **Melson et al., 2002**) are reported in **Table S2**.

In situ trace element analyses by LA-ICP-MS at Clermont-Ferrand.

Trace element analyzes on the EX1702-D3-2 glass sample were made using a laser ablation ICP-MS system housed at Laboratoire Magmas et Volcans at Clermont-Ferrand. Analytical methods are outlined in Oulton et al. (2016) and Reinhart et al. (2018). Analyses were made using a Thermo Scientific Element XR ICP-MS coupled to a Resonetics M-50E 193 nm ArF excimer laser. <sup>43</sup>Ca was used as an internal standard. All surfaces were preablated (for 1s at 10Hz) prior to analysis. Analyses of samples and standards used a 47 µm laser spot, and the laser was fired with a 4 Hz repetition rate. Analyses were conducted over 80 second ablation periods, with 20 seconds of blank analysis (with the laser off) before samples analysis and (following a washout period) 20 seconds of blank analysis (again, with the laser off) after the analysis. Analyses were made in low resolution mode using triple mode with a 20% mass window and a 20 ms integration window. Acceleration voltage was scanned between magnet scans to ensure peak positions were maintained. Calibration curves were generated using NIST612 (Gagnon et al., 2008) and BCR-2 (Jochum et al., 2006) glass. Replicate analyses of a MORB glass, 519-4-1, were made throughout the analytical session to monitor precision and accuracy of analyses. The reproducibility of the trace element analyses was better than 10% (2RSD, N=8) for all elements except for Cs (44%). Measured concentrations are compared with previously published analyses from Gale et al. (2013) in Table S2.

## <sup>40</sup>Ar/<sup>39</sup>Ar Geochronology at Oregon State University

Clinopyroxene separates were prepared from basalt samples AVON-D66-1 (Rose atoll) and EX1702-D7-2 (Moki) following the methods outlined in Konrad et al. (2019). Separate gases were processed and analyzed on a new extraction line and ARGUS VI mass spectrometer housed at Oregon State University. Incremental heating experiments consisted of 20-21 steps using a CO<sub>2</sub> laser. Blanks were analyzed at the experiment start, end and between every three heating steps. Gas was processed and analyzed using the same methods outlined for the ARGUS-VI-E in Konrad et al. (2019). ArArCalc v.2.7.0 (Koppers, 2002) was used to process results and calculate age determinations. A Fish Canyon Tuff fluence monitor age of 28.201  $\pm$  0.046 Ma (2 $\sigma$ ; Kuiper et al., 2008) and a total decay constant of 5.530  $\pm$  0.097  $\times$  10 $^{-10}$  year $^{-1}$  (2 $\sigma$ ; Min et al., 2000) were used to calculate the ages.

### **References Cited**

- Beguelin, P., M. Bizimis, C. Beier, and S.Turner, 2017, Rift–plume interaction reveals multiple generations of recycled oceanic crust in Azores lavas. *Geochimica et Cosmochimica Acta*, v. 218, p. 132–152.
- Eisele, J., Abouchami, W., Galer, S.J.G., and Hofmann, A.W., 2003, The 320 kyr Pb isotope evolution of Mauna Kea lavas recorded in the HSDP-2 drill core. *Geochemistry, Geophysics, Geosystems*, v. 4, 8710, doi:10.1029/2002GC000339.
- Frisby, C., Bizimis, M. and Mallick, S., 2016, Hf–Nd isotope decoupling in bulk abyssal peridotites due to serpentinization. *Chemical Geology*, v. 440, p. 60-72.
- Gagnon, J.E., Fryer, B.J., Samson, I.M., Williams-Jones, A.E., 2008, Quantitative analysis of silicate certified reference materials by LA-ICPMS with and without an internal standard. *Journal of Analytic Atomic Spectrometry*, v. 23, p. 1529–1537.

- Gale, A., M. Laubier, S. Escrig, and C. H. Langmuir, 2013, Constraints on melting processes and plume-ridge interaction from comprehensive study of the FAMOUS and North Famous segments, Mid-Atlantic Ridge. *Earth and Planetary Science Letters*, v. 365, p. 209–220, doi:10.1016/801j.epsl.2013.01.022.
- Garçon, M., Boyet, M., Carlson, R.W., Horan, M.F., Auclair, D., and Mock, T.D., 2018, Factors influencing the precision and accuracy of Nd isotope measurements by thermal ionization mass spectrometry. *Chemical Geology*, v. 476 p. 493–514.
- Hart, S.R., and Blusztajn, J., 2006, Age and geochemistry of the mafic sills, ODP site 1276, Newfoundland margin. *Chemical Geology*, v. 235, p. 222–237.
- Jackson, M.G., Hart, S.R., Konter, J.G., Koppers, A.A.P., Staudigel, H., Kurz, M.D., Blusztajn,
   J., and Sinton, J.M., 2010, The Samoan hotspot track on a "hotspot highway":
   Implications for mantle plumes and a deep Samoan mantle source. *Geochemistry, Geophysics, Geosystems*, v. 11, Q12009, doi:10.1029/2010GC003232.
- Jackson, M.G., Koga, K.T., Price, A., Konter, J.G., Koppers, A.A.P., Finlayson, V.A., Konrad, K., Hauri, E.H., Kylander-Clark, A., Kelley, K.A., and Kendrick, M.A., 2015, Deeply-dredged submarine HIMU glasses from the Tuvalu Islands, Polynesia: Implications for volatile budgets of recycled oceanic crust. *Geochemistry, Geophysics, Geosystems*, v. 16, p. 3210-3234, DOI: 10.1002/2015GC005966.
- Jackson, M.G., Halldórsson, S.A., Price, A., Kurz, M.D., Konter, J.G., Koppers, A.A.P., Day, J.M.D., 2020, Contrasting old and young volcanism from Aitutaki, Cook Islands: Implications for the origins of the Cook-Austral volcanic chain. Journal of Petrology, egaa037, https://doi.org/10.1093/petrology/egaa037.
- Jochum, K., Stoll, B., Herwig, K., Willbold, M., Hofmann, A., Amini, M., Aarburg, S., Abouchami, W., Hellebrand, E., Mocek, B., Raczek, I., Stracke, A., Alard, O., Bouman, C., Becker, S., Dücking, M., Brätz, H., Klemd, R., Bruin, D., Canil, D., Cornell, D., Hoog, C.-J., Dalpe, C., Danyushevsky, L., Eisenhauer, A., Gao, Y., Snow, J., Groschopf, N., Günther, D., Latkoczy, C., Guillong, M., Hauri, E., Höfer, H., Lahaye, Y., Horz, K., Jacob, D., Kasemann, S., Kent, A., Ludwig, T., Zack, T., Mason, P., Meixner, A., Rosner, M., Misawa, K., Nash, B., Pfänder, J., Premo, W., Sun, W., Tiepolo, M., Vannucci, R., Vennemann, T., Wayne, D., and Woodhead, J., 2006, MPIDING reference glasses for in situ microanalysis: new reference values for element concentrations and isotope ratios. *Geochemistry, Geophysics, Geosystems*, v. 7, Q02008.
- Jochum, K., Weis, U., Schwager, B., Stoll, B., Wilson, S.A., Haug, G.H., Andreae, M.O., Enzweiler, J., 2016, Reference values following ISO guidelines for frequently requested rock reference materials. *Geostandards and Geoanalytical Research*, v. 40, p. 333-350.
- Johnson, D.M., Hooper, P.R., and Conrey, R.M., 1999, XRF analysis of rocks and minerals for

- major and trace elements in a single low dilution Li-tetraborate fused bead. *Advances in X-Ray Analysis*, v. 41, p. 843–867.
- Knaack, C.M., Cornelius, S.B., and Hooper, P.R., 1994, Trace element Analysis of rocks and minerals by ICP-MS. Open File Report, GeoAnalytical Lab. Washington State University, p. 10.
- Koppers, A. A., 2002. ArArCALC—software for 40Ar/39Ar age calculations. Computers & Geosciences, v. 28, p. 605-619.
- Konrad, K., Koppers, A. A., Balbas, A. M., Miggins, D. P., & Heaton, D. E., 2019. Dating clinopyroxene phenocrysts in submarine basalts using 40Ar/39Ar geochronology. Geochemistry, Geophysics, Geosystems, v. 20, p. 1041-1053.
- Kuiper, K., Deino, A., Hilgen, F., Krijgsman, W., Renne, P., & Wijbrans, J., 2008. Synchronizing rock clocks of Earth history. Science, v. 320, p. 500-504.
- McDonough, W.F., Sun, S.S., 1995, The composition of the Earth. *Chemical Geology*, v. 120, p. 223-253.
- Melson, W.G., O'Hearn, T., and Jarosewich, E., 2002, A data brief on the Smithsonian Abyssal Volcanic Glass Data File. *Geochemistry, Geophysics, Geosystems*, v. 3, p. 1-11, doi:10.1029/2001GC000249.
- Min, K., Mundil, R., Renne, P. R., and Ludwig, K. R., 2000. A test for systematic errors in <sup>40</sup>Ar/<sup>39</sup>Ar geochronology through comparison with U/Pb analysis of a 1.1-Ga rhyolite. Geochimica et Cosmochimica Acta, v. 64, p. 73–98. https://doi.org/10.1016/S0016-7037(99)00204-5
- Munker, C., Weyer, S., Scherer, E. and Mezger, K., 2001, Separation of high field strength elements (Nb, Ta, Zr, Hf) and Lu from rock samples for MC-ICPMS measurements. *Geochemistry, Geophysics, Geosystems*, v. 2, p. 1064, doi:10/1029:2001GC000183.
- Oulton, J., Humayun, M., Fedkin, A., and Grossman, L., 2016, Chemical evidence for differentiation, evaporation and recondensation from silicate clasts in Gujba. *Geochimica et Cosmochimica Acta*, v. 177, p. 254–274.
- Price, A.A., Jackson, M.G., Blichert-Toft, J., Hall, P.S., Sinton, J.M., Kurz, M.D., and Blusztajn, J., 2014, Evidence for a broadly distributed Samoan-plume signature in the northern Lau and North Fiji Basins. *Geochemistry, Geophysics, Geosystems*, v. 15, p. 986-1008, doi: 10.1002/2013GC005061.
- Price, A.A., Jackson, M.G., Blichert-Toft, J., Blusztajn, J., Conatser, C.S., Konter, J.G., Koppers, A.A.P., and Kurz, M.D., 2016, Geochemical evidence in the Northeast Lau Basin for subduction of the Cook-Austral volcanic chain in the Tonga Trench. *Geochemistry, Geophysics, Geosystems*, v. 17, p. 1694-1724, doi:10.1002/2015GC006237.

- Reinhard, A.A., Jackson, M.G., Koornneef, J.M., Rose-Koga, E.F., Blusztajn, J., Konter, J.G., Koga, K.T., Wallace, P.J., Harvey, J., 2018, Sr and Nd isotopic compositions of individual olivine-hosted melt inclusions from Hawai'I and Samoa: Implications for the origin of isotopic heterogeneity in melt inclusions from OIB lavas. *Chemical Geology*, v. 495, p. 36-49.
- Tanaka, T., Togashi, S., Kamioka, H., Amakawa, H., Kagami, H., Hamamoto, T., Yuhara, M.,
  Orihashi, Y., Yoneda, S., Shimizu, H., Kunimaru, T., Takahashi, K., Yanagi, T., Nakano,
  T., Fujimaki, H., Shinjo, R., Asahara, Y., Tanimizu, M., and Dragusanu, C., 2000, JNdi1: A neodymium isotopic reference in consistency with LaJolla neodymium. *Chemical Geology*, v. 168, p. 279–281.
- Weis, D., Kieffer, B., Maerschalk, C., Barling, J., de Jong, J.. Williams, G.A., Hanano, D., Pretorius, W., Mattielli, N., Scoates, J.A., Goolaerts, A., Friedman, R.M., Mahoney, B.J., 2006, High-precision isotopic characterization of USGS reference materials by TIMS and MC-ICP-MS. *Geochemistry, Geophysics, Geosystems*, v. 7, Q08006.
- Weis, D., Kieffer, B., Hanano, D., Silva, I.N., Barling, J., Pretorius, W., Maerschalk, C., Matielli, N., 2007, Hf isotope compositions of U.S. Geological Survey reference materials. *Geochemistry, Geophysics, Geosystems*, v. 8, Q06006.
- Wessel, P., and Kroenke, L.W., 2008, Pacific absolute plate motion since 145Ma: an assessment of the fixed hot spot hypothesis. *Journal of Geophysical Research*, v.113, B06101. https://doi.org/10.1029/2007JB005499.
- White, W.M., Albarede, F. and Telouk, P., 2000, High-precision analysis of Pb isotope ratios by multi-collector ICP-MS. *Chemical Geology*, v. 167, p. 257-270.

## **Figure Captions**

Figure S1. Isotopic data for volcanoes in this study plotted with existing data for Macdonald and Arago volcanoes. The Moki and Malulu isotopic data produced for this study are from clinopyroxene phenocrysts, as seawater alteration prevented the analysis of whole rock samples. New data also include pillow rim glass analyses from Rose atoll, whole rock data from Dino seamount, and new whole rock data on Rose and Malulu lavas. Whole rock data for the Rose atoll and the Malulu and Papatua seamounts was published by Jackson et al. (2010). Young (Cook-Austral) Arago and Macdonald isotope fields are represented by red and blue backgrounds, respectively, and solid outlines. Old (Cretaceous) Arago and Macdonald fields are represented by light and dark gray fields with long and short dashed outlines, respectively. <sup>143</sup>Nd/<sup>144</sup>Nd data from sample SUA-1 (Konter et al., 2008) is not shown due to relatively large measurement errors ( $\pm$  195 ppm). The Tuvalu, Gilbert, Marshall and Wake islands and seamounts define the older portion of the Arago hotspot (data sources from Staudigel et al., 1991; Konter et al., 2008; Finlayson et al., 2018; Konrad et al., 2018); the Tokelau Islands and seamounts define the older portion of the Macdonald hotspot (data sources from Konter et al., 2008). Measured isotopic values are shown, but where <sup>40</sup>Ar/<sup>39</sup>Ar ages are available (Moki, Rose atoll), an age correction to the time of eruption is calculated. The isotopic change due to the age correction is shown by the line extending from the respective datapoints (which represents the magnitude and direction of the age correction). The other samples (Malulu, Papatua, and Dino) are not associated with ages and age corrections are not provided. All data not produced by this study was previously published and downloaded from Georoc (http://georoc.mpch681mainz.gwdg.de/georoc). Figure modified after Jackson et al. (2020).

Figure S2. Trace element spider diagrams for whole rock and clinopyroxene samples from study volcanoes. Trace element concentrations are normalized to pyrolite from McDonough and Sun (1995). Whole rocks are shown in the top panel, and clinopyroxenes in the lower panel.

**Figure S3:** Age plateaus and inverse isochrons for clinopyroxene (CPX) separates from AVON-66-1 (Rose Atoll; left panel) and EX1702-D7-2 (Moki Seamount; right panel). The Rose Atoll sample is a combined incremental heating result for a 355-500 μm size fraction (blue) and a 500-595 μm size fraction (orange), which is justified because both plateau ages are concordant; the plateau age is adopted for the Rose age determination. A single heating experiment is presented for the Moki Seamount clinopyroxene (cpx) that contained very low concentrations of K and corresponding radiogenic gas, resulting in high individual step uncertainties, particularly for the first two heating steps. The lines above the plateaus represent steps used in the age calculation, and all steps were incorporated into the respective ages. Inverse isochrons are shown beneath the plateau panels for each analysis. Black squares represent points used in the calculations while white squares represent excluded points. The inverse isochron age determination is preferred (for Moki) due to the slightly above atmospheric <sup>40</sup>Ar/<sup>36</sup>Ar<sub>int</sub> value. Both measurements meet standard <sup>40</sup>Ar/<sup>39</sup>Ar quality criteria with plateaus consisting of >60% cumulative <sup>39</sup>Ar(K), appropriate mean-square of weighted deviants (MSWD) and probability-of-fit (P) values greater than 0.05 (see Supplemental Tables 3 and 4).

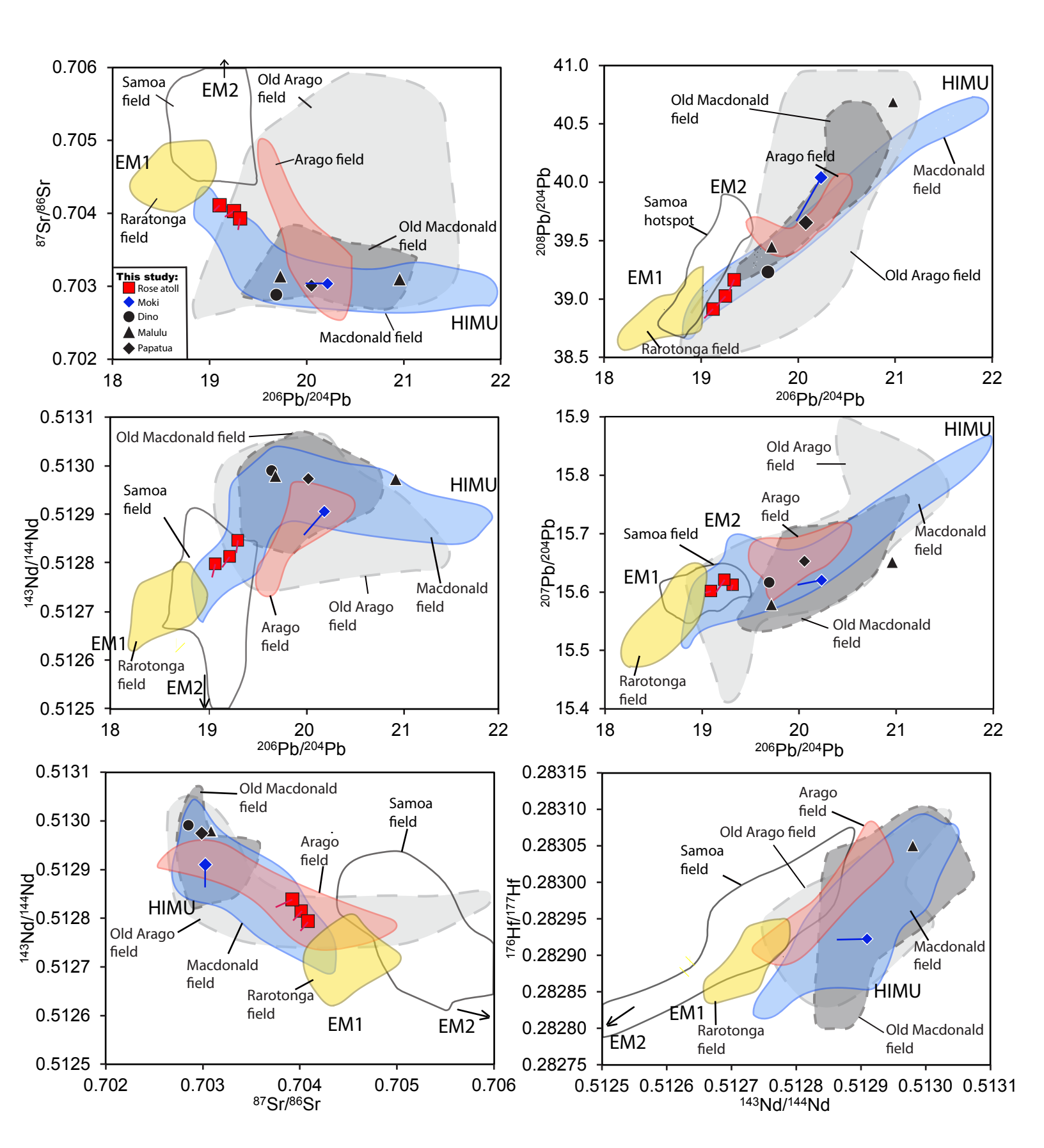
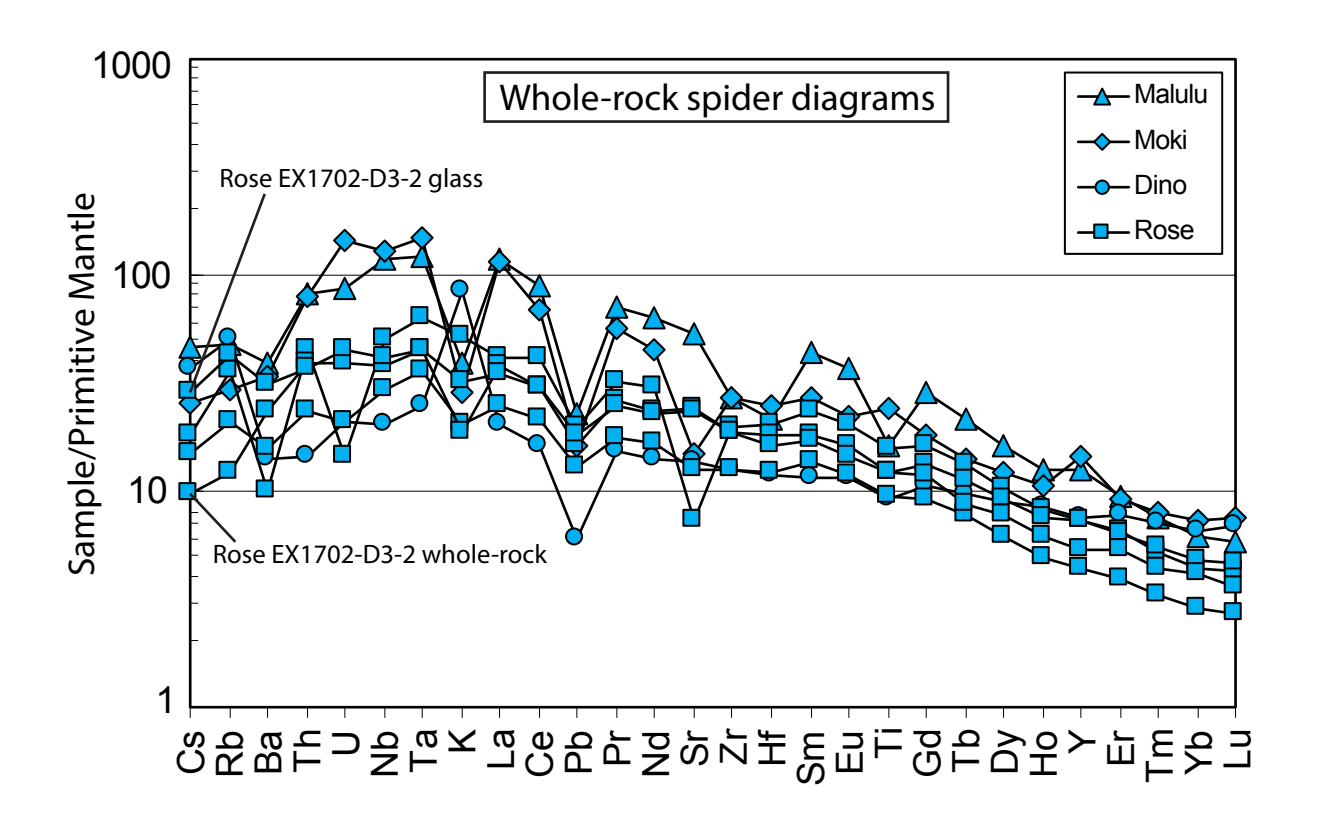


Figure S1



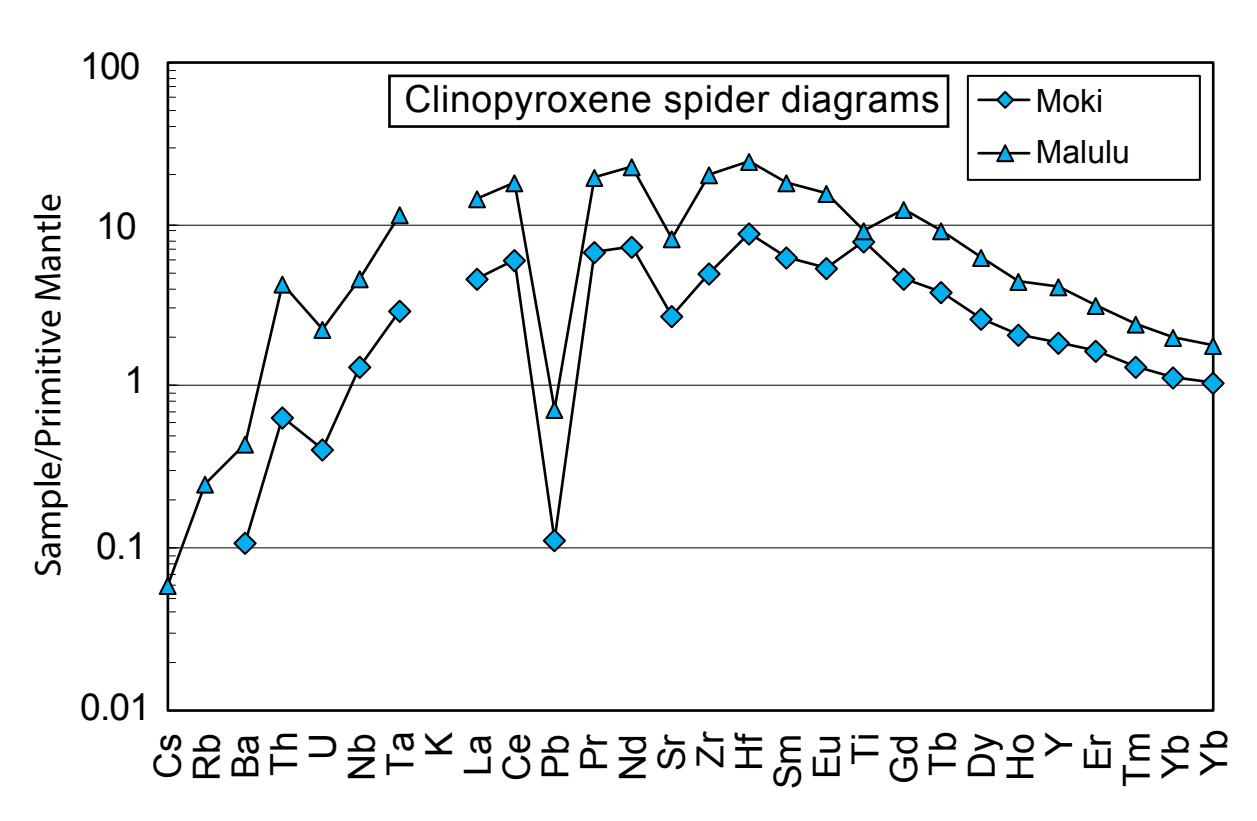


Figure S2

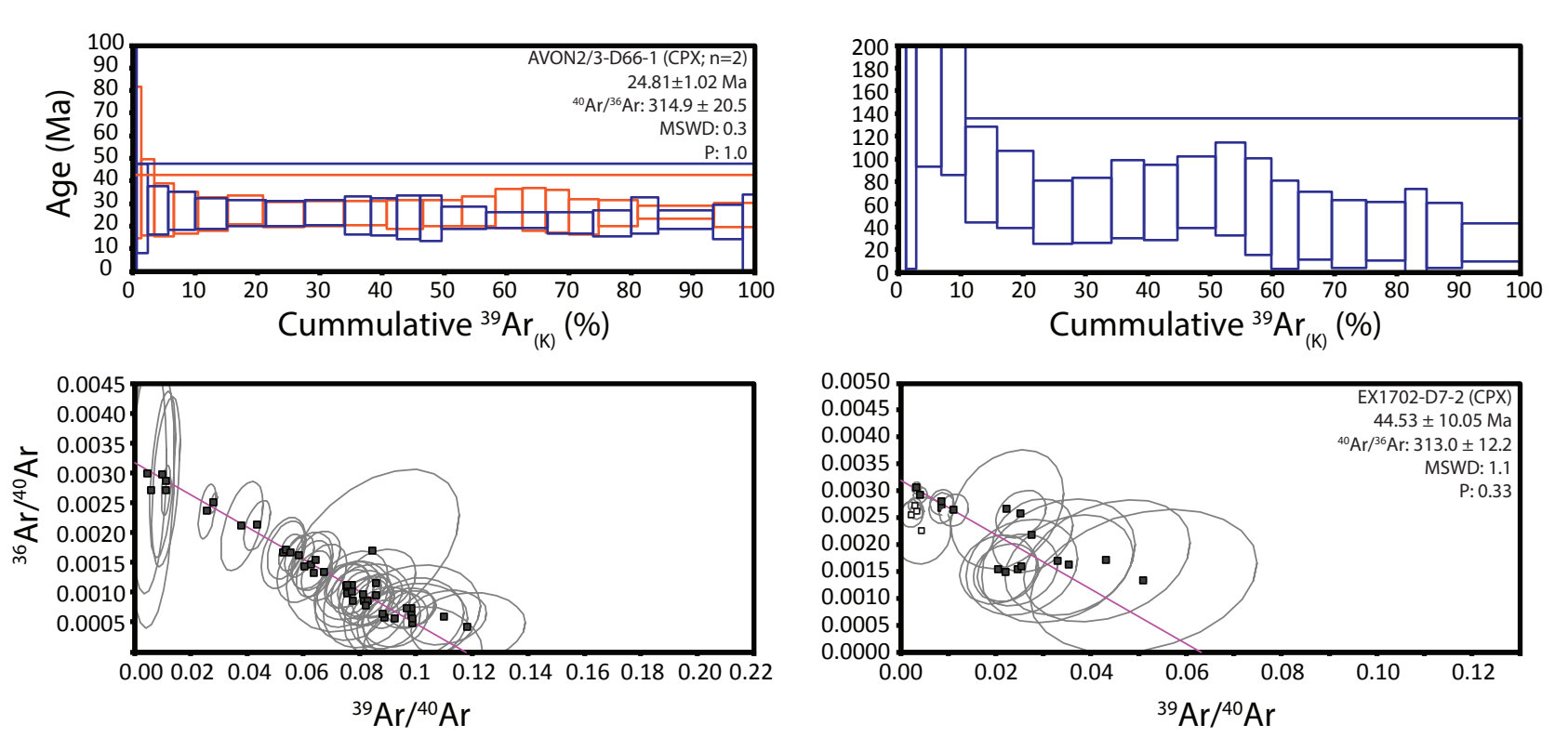


Figure S3